AIAA 2003–4262

Model-based control of vortex shedding using low-dimensional Galerkin models

J. Gerhard, M. Pastoor, R. King
Measurement and Control Group,
Institute for Process and Plant Technology,
Technical University of Berlin, Berlin, GERMANY

B.R. Noack, A. Dillmann
Hermann-Föttinger-Institute of Fluid Mechanics,
Technical University of Berlin, Berlin, GERMANY

M. Morzyński
Institute of Combustion Engines and Basics of Machine Design,
Poznań University of Technology, Poznań, POLAND

G. Tadmor
Department of Electrical and Computer Engineering,
Northeastern University, Boston, MA, U.S.A.

33rd AIAA Fluids Conference & Exhibit
June 23 – 26, 2003
Orlando, Florida

MODEL-BASED CONTROL OF VORTEX SHEDDING USING LOW-DIMENSIONAL GALERKIN MODELS

Johannes Gerhard*, Mark Pastoor†, Rudibert King‡
Measurement and Control Group, Institute for Process and Plant Technology, Technical University of Berlin P2-1
Hardenbergstraße 36a, D-10623 Berlin, Germany

Bernd R. Noack§, Andreas Dillmann¶
Hermann-Föttinger-Institute of Fluid Mechanics, Technical University of Berlin HF1
Straße des 17. Juni 135, D-10623 Berlin, Germany

Marek Morzyński‖
Institute of Combustion Engines and Basics of Machine Design, Poznań University of Technology
ul. Piotrowo 3, PL 60-965 Poznań, Poland

Gilead Tadmor**
Department of Electrical and Computer Engineering, Northeastern University
440 Dana Research Building, Boston, MA 02115, U.S.A.

Abstract

A model-based flow control strategy is proposed for the suppression of vortex shedding behind a circular cylinder. The control design is based on a hierarchy of low-dimensional Galerkin models of the cylinder wake. These models are constructed from a Karhunen-Loève decomposition of a simulation without actuation. The key enablers are an additional physical mode in the Karhunen-Loève approximation and an energy-based control which respects the regime of model validity. The developed control strategy is successfully tested in direct numerical simulations.

*Research engineer. Corresponding author: phone: ++49-30-314.79574, x24100; fax: x21129; e-mail: johannes.gerhard@tu-berlin.de
†Research engineer
‡Professor
§Research engineer
¶Professor
‖Professor
**Associate Professor

I Introduction

Real time capability requires simplicity of the control law and is, hence, difficult to obtain from a high-dimensional direct numerical simulation (DNS) or a large eddy simulation (LES). This requirement generally excludes feedback design based on such models, for instance, in computationally expensive optimal control strategies for Navier-Stokes solvers.[1] Control designs based on low-dimensional flow models aim to address the complexity issue. Examples of low-dimensional representations include vortex models[2,3] and Galerkin models (GM),[4,5] both of which can be considered as a test-bed for the physical understanding of the flow. The simple controller proposed in this paper is derived from an energy-dynamics analysis in a low-dimensional GM, and is successfully verified with a DNS.

The suppression of laminar vortex shedding behind a circular cylinder is chosen as a bench-mark problem for the presented strategy. This problem has been extensively investigated for several decades. Proposed suppression techniques include passive means, like splitter plates[6] and small control cylinders,[7] active means, e.g. jet bleed[8] or acoustic excitation,[9] and closed-loop control with acoustic actuation and hot-wire signals.[10] In the current

study, actuation is provided by a local volume force in the near-wake (see Fig. 1). This force mimics, for instance, a Lorentz force in a magneto-hydrodynamical flow. The reduction of the fluctuation level is monitored in a near-wake observation region, since global suppression of the vortex street with a local volume force cannot be expected. The observation region extends up to six diameters downstream of the cylinder and is bounded by the streamwise position of the velocity measuring sensor.

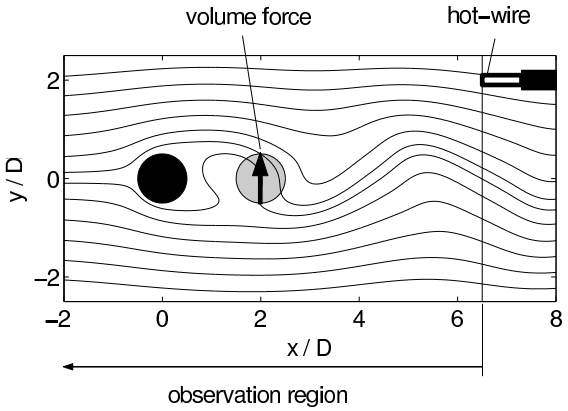

Figure 1: *Stream-lines of the natural flow around a circular cylinder (solid circle) with the diameter $D = 1$. The direction and domain of the volume force is illustrated by an arrow and a circle, respectively. The hot-wire anemometer is located at a typical experimental position. Success of control is monitored in the observation region bounded by the streamwise position of the sensor.*

The empirical GM used here is based on a Karhunen-Loève decomposition of an unforced reference simulation. The volume force is incorporated in the GM. The reference Reynolds number of 100 is in the laminar shedding regime and far above the critical Reynolds number[11] of 47 and small enough to exclude transition.[12]

The paper is organized as follows: In Sec. II, a hierarchy of GMs is introduced. In Sec. III, the control strategy with DNS tests is described. The results are discussed in Sec. IV. The main findings are summarized in Sec. V together with an outlook.

II Galerkin models

A hierarchy of models of the natural and the actuated flow is introduced in this section. A direct numerical simulation of the flow is presented first. Snapshots of this simulation constitute the fundament for low-dimensional GMs. The issues of energy resolution and model validity over a dynamic range are addressed in the model development.

II.1 Direct numerical simulation

The flow is described in a Cartesian coordinate system x, y, where the x-direction is aligned with the flow and the y-direction is orthogonal to the flow and to the cylinder axis. The origin is in the center of the cylinder. The time is represented by t. The velocity and pressure fields are denoted by $\mathbf{u}$ and p, respectively. All quantities are assumed to be non-dimensionalized with the velocity of the flow U, the diameter of the cylinder D, and the density of the fluid ρ.

GM construction starts with a well-resolved DNS solution of the non-dimensional incompressible Navier-Stokes equation,

$$\partial_t \mathbf{u} + \nabla \cdot (\mathbf{u}\,\mathbf{u}) = -\nabla p + \nu \Delta \mathbf{u} + G\,\mathbf{g}, \quad (1)$$

where ν is the reciprocal of the Reynolds number and $\mathbf{g}$ represents a steady local force field in the y-direction. The forcing amplitude G is a time-dependent control input. The volume force has compact support in a circular region which is centered two diameters downstream from the cylinder (see Fig. 1) and which has the same diameter as the cylinder.

The computational domain of the direct simulation is the rectangular region

$$\Omega := \{(x,y) : -5 \le x \le 15,\ |y| \le 5\}. \quad (2)$$

The flow is discretized as finite elements on an unstructured triangular mesh. The finite-element Navier-Stokes solver is of cubic accuracy in space and time and employs pseudo-pressure formulation.[13]

II.2 Energy-resolving models

The goal of the empirical Galerkin modeling is to reproduce the Navier-Stokes simulation in a low-dimensional manner. The GM is based on a generalized Karhunen-Loève expansion around an (unstable) steady Navier-Stokes solution $\mathbf{u}_s$ with Karhunen-Loève modes $\mathbf{u}_i$, $i = 1, \ldots, N$ and a so called shift-mode $\mathbf{u}_\Delta$,[14,15]

$$\mathbf{u}^{[N]} = \mathbf{u}_s + \sum_{i=1}^{N} a_i\,\mathbf{u}_i + a_\Delta\,\mathbf{u}_\Delta. \quad (3)$$

The modes $\mathbf{u}_s$, $\mathbf{u}_i$, $i = 1, \ldots, N$ and $\mathbf{u}_\Delta$ are defined in the whole computational domain Ω. Their velocity fields depend only on the location $\mathbf{x}$, and the time-dependence is described by the Fourier coefficients a_1, ..., a_N, a_Δ. The Karhunen-Loève modes

are obtained with the snapshot method[4] from the post-transient periodic wake solution. The modes are visualized in Fig. 2.

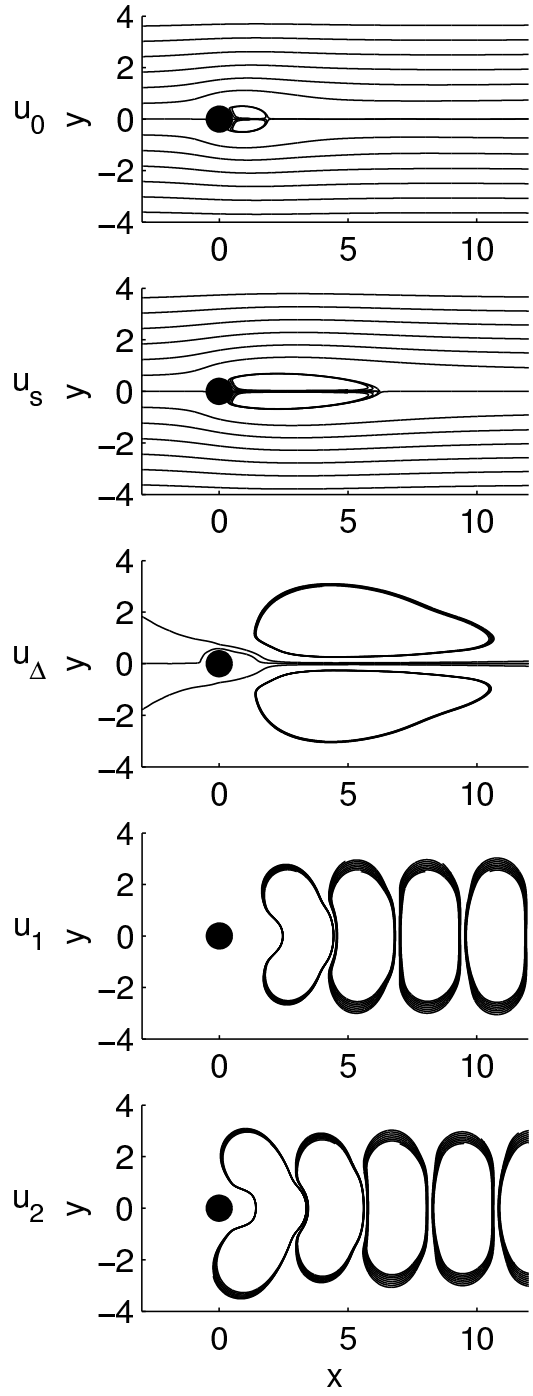

Figure 2: *Galerkin approximation. The mean flow* $\mathbf{u_0}$*, the steady solution* $\mathbf{u}_s$*, the shift-mode* $\mathbf{u}_\Delta$*, and the Karhunen-Loéve modes* $\mathbf{u}_1$*,* $\mathbf{u}_2$ *are visualized (top to bottom) with stream-lines.*

The Galerkin approximation (GA) (3) includes:

(i) the steady solution $\mathbf{u}_s$, as the origin of the state space: $a_1 = \ldots = a_N = a_\Delta = 0$,

(ii) the mean flow, $\mathbf{u}_0 = \mathbf{u}_s + a_\Delta \mathbf{u}_\Delta$, with suitable a_Δ, i.e. $a_i = 0$, $i = 1, \ldots, N$,

(iii) the periodic von Kármán vortex street, as a limit cycle, and

(iv) the transient from the steady solution to the limit cycle.

Empirical GMs typically deteriorate rapidly as the system departs from the trajectory used for model construction.[16] The inclusion of the shift-mode enables a representation of variations in the mean flow and is critical for extending an improved representation of transients. Therefore, the shift-mode is the key enabler for the presented model hierarchy and the robustness of the GM. The amplitude of this mode is also used in a proportional and differential feedback control strategy of the cylinder wake which is forced by transverse displacement of the cylinder.[17]

The GA with $N = 2$ resolves the first harmonics of the natural flow corresponding to some 96% of its fluctuation energy. The remaining 4% of the fluctuation energy are nearly completely resolved by the next six Karhunen-Loève modes. Thus, a GM with eight Karhunen-Loève modes and the shift-mode yields an accurate reproduction of the natural flow.

The Galerkin projection (GP) of the Navier-Stokes equation (1) over the subspace spanned by the GA (3) yields a Galerkin system (GS) of ordinary differential equations $da_i/dt = f_i(a_1, \ldots, a_N, a_\Delta, G)$, governing the temporal evolution of the Fourier coefficients. The formalism is simplified by the notation $a_0 := 1$ and $a_{N+1} := a_\Delta$, and the use of an Einstein summation convention, where double indices j, k imply summation over $0, 1, \ldots, N+1$ and i runs over $1, \ldots, N+1$. Then, the GS is expressed by

$$\frac{d}{dt} a_i = \nu \, l_{ij} \, a_j + q_{ijk} \, a_j \, a_k + G \, g_i, \qquad (4)$$

where the linear term, $l_{ij}\, a_j$, originates from the GP of the viscous term, $\nu \Delta \mathbf{u}$, and the quadratic term, $q_{ijk} a_j a_k$, from the GP of the convective term $\nabla \cdot (\mathbf{u}\,\mathbf{u})$. The pressure term can be neglected in a sufficiently large computational domain.[16]

The transient phase of the first two Fourier coefficients a_1 and a_2 and the shift-mode amplitude a_Δ from the steady solution to the limit cycle is shown in Fig. 3.

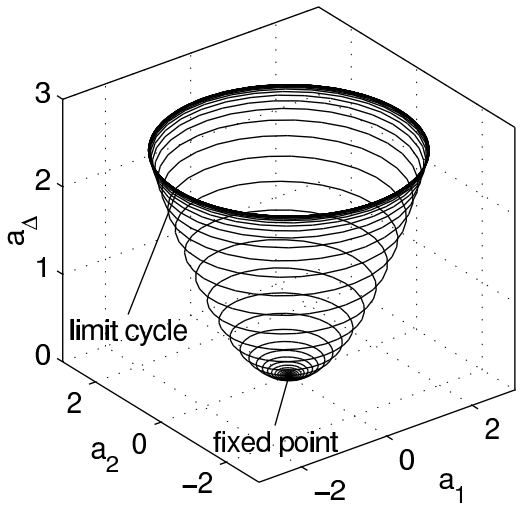

Figure 3: *Transient from the steady solution to the limit cycle in state space. The solution defined by $a_1(t)$, $a_2(t)$, and the shift-mode amplitude $a_\Delta(t)$ stays on a paraboloid. The fixed point is given by $a_1 = a_2 = a_\Delta = 0$ and the limit cycle is approximated by $a_1^2 + a_2^2 = A^2 = const$ and $a_\Delta = const$.*

II.3 Minimal model

The minimal model includes the first pair of Karhunen-Loève modes ($N = 2$) and the shift-mode, i.e. the state space is spanned by a_1, a_2 and $a_3 := a_\Delta$. The main characteristics of the flow is reproduced by the minimal model. It resolves the von Kármán vortex street moving downstream from the cylinder and neglects the higher harmonics.

II.4 Phase-invariant model

For control design, the minimal model is further reduced with a simple mean-field-type approximation.[18,19] The Bogoliubov-Krylov ansatz, employed in mean-field theory approximates the Fourier coefficients by $a_1 = A\cos(\phi)$, $a_2 = A\sin(\phi)$. Here, A, a_Δ, and the frequency $\omega = d\phi/dt$, are assumed to be slowly varying functions of time, as compared to the oscillation period. Thus, the GS (4) reduces to the following phase-invariant equations in cylindrical coordinates:

$$\frac{d}{dt}A = (\sigma_A - \beta a_\Delta)A + F_A\,, \qquad (5a)$$

$$\frac{d}{dt}\phi = \omega_s + \gamma a_\Delta + F_\phi\,, \qquad (5b)$$

$$\frac{d}{dt}a_\Delta = -\sigma_\Delta a_\Delta + cA^2\,, \qquad (5c)$$

where $\omega = \omega_s + \gamma a_\Delta$ is a state-dependent representation of the instantaneous oscillation frequency. Here, ω_s represents the predicted initial frequency near the fixed point and γ quantifies the change of the frequency the variation of the mean flow. The forcing terms F_A in Eq. (5a) and F_ϕ of Eq. (5b) are given by

$$F_A = G(g_1\cos(\phi) + g_2\sin(\phi))\,, \qquad (6a)$$

$$F_\phi = \frac{G}{A}(-g_1\sin(\phi) + g_2\cos(\phi))\,. \qquad (6b)$$

The time-constant of the shift-mode, $T_\Delta = 1/\sigma_\Delta$ is significantly smaller than the one of the period of oscillation T, i.e. $T \ll T_\Delta$. Hence, the time derivative of a_Δ can be neglected and a_Δ is slaved to the oscillation amplitude A by $a_\Delta \approx (c/\sigma_\Delta)\,A^2$.

Figure 4 shows the limit-cycle attractor of the three models in comparison with the simulation. The amplitude of the energy-resolving model is a good approximation of the simulation. The amplitude predicted by the minimal model is too large. This overprediction is a result of the neglected energy transfer from the first harmonic to higher harmonic modes. The assumption of phase invariance has only little effect on the limit cycle since the ansatz for a_1 and a_2 is a very good approximation of real conditions.

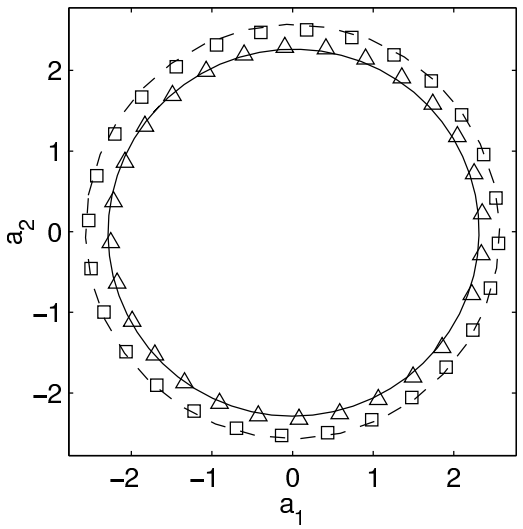

Figure 4: *Simulated and modeled attractor of the periodic flow. The figure displays a phase-portrait with the Fourier coefficients $a_1(t)$, $a_2(t)$ of the energy-resolving (△), minimal (□), and phase-invariant model (−−) as compared with the simulation (—).*

III Model-based flow control

In this section, the control design is described. Following the outline in Sec. III.1, an energy-based control is proposed in Sec. III.2, and observer design is discussed in Sec. III.3. Closed-loop simulation results are presented in Sec. III.4. In order to asses the efficiency of an observer-based control, its response is compared with those obtained with a complete-information control in Sec. III.5, and with a passive splitter-plate in Sec. III.6.

III.1 Outline

The control structure is outlined in Fig. 5 for the minimal GM.

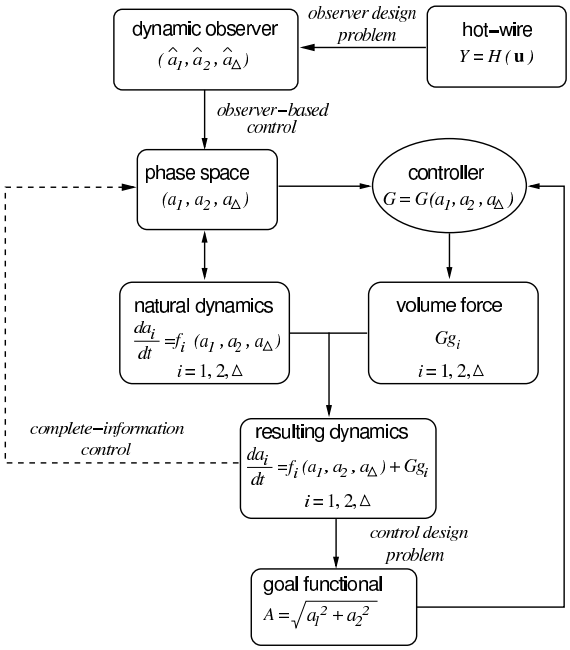

Figure 5: *Outline of control structure in the design phase.*

The state of the flow is described by the GA, i.e. by the three Fourier coefficients $\mathbf{a} = (a_1, a_2, a_\Delta)$. The control goal is to minimize the oscillation amplitude $A = \sqrt{a_1^2 + a_2^2}$, targeting $A = 0$ as the ideal steady state. Given the steady state equality $a_\Delta = (c/\sigma_\Delta)\, A^2$, this objective is equivalent to the stabilization of the origin in the state space of Eq. (4). In the *complete-information design task*, the control input (i.e. the volume-force amplitude G) to stabilize Eq. (4) has to be selected as a function of the velocity field $\mathbf{u}$, hence of the full state (a_1, a_2, a_Δ). In an *observer-based control*, available information is limited to the single measured velocity signal, Y, which can be considered as a function of the velocity field, $H(\mathbf{u})$. The *observer design problem* consists of reconstructing the state vector from the measured velocity signal.

An important aspect of control design — for systems such as this — is a recognition of the limitation of the model, e.g. its domain of validity. The range of validity of the low-dimensional model used here is the domain in which it provides a good approximation of actual dynamics and is limited to a tight neighborhood of the center manifold visualized in Fig. 3. An additional restriction is the preservation of the oscillatory solution with the natural Strouhal number. Unless special attention is paid to this point, a typical control theoretical equilibrium stabilization would lead to solutions which are likely to leave the range of validity of the GM, and therefore cannot be successfully implemented in a Navier-Stokes simulation, let alone the physical system. A control strategy which preserves the range of model validity is described in the following section.

III.2 Energy-based controller

The goal of the energy-based controller is to achieve a continuous decay rate σ of the fluctuation energy until steady state is reached — leaving the frequency ω nearly unaltered.

A simple and energy efficient realization is $G = -G_0$ if $g_1 \cos(\phi) + g_2 \sin(\phi) > 0$ and $G = +G_0$ otherwise. The amplitude G_0 is determined once every period in agreement with the desired decay rate. The mean impact of the force on the frequency is small because of the sign-change of the angle force-term F_ϕ (see Eq. (6b)) during the time of constant force direction. Details and improvements of this control are described by Tadmor *et al.*[20]

III.3 Observer design

Observer design is needed for just about any experimental realizations of flow control. In the current system, only one or two hot-wire signals may be implementable with small interference with the flow. Hence, a measurement of the Fourier coefficients of distributed modes is utterly impossible in a real-time implementation. The reconstruction of the state vector from a sensor signal is performed with a dynamic observer. The observer duplicates the original phase-invariant model (5), with an additional

correction term $\mathbf{L}\,\Delta Y$:

$$\frac{d}{dt}\hat{A} = (\sigma_A - \beta\hat{a}_\Delta)\hat{A} + F_A + L_A\Delta Y\,, \quad (7a)$$

$$\frac{d}{dt}\hat{\phi} = \omega_s + \gamma\hat{a}_\Delta \quad + F_\phi + L_\phi\Delta Y\,, \quad (7b)$$

$$\frac{d}{dt}\hat{a}_\Delta = -\sigma_\Delta\hat{a}_\Delta + c\hat{A}^2 \quad + L_\Delta\Delta Y\,, \quad (7c)$$

where the hat symbol denotes an estimated state variable. The measurement estimation error is defined by $\Delta Y := Y - \hat{Y}$, where $\hat{Y}$ is a function of the estimated Galerkin state space, $\hat{H}(\hat{\mathbf{a}})$. This error has two major sources, the assumed initial condition and differences between the real flow and the reduced order phase-invariant model. Design of the gain matrix $\mathbf{L}$ is based on the stabilization of the linearized dynamics of the state-space estimation error $\Delta\mathbf{a} := \mathbf{a} - \hat{\mathbf{a}}$.

The combined estimation error e of the oscillating Fourier coefficients a_1 and a_2

$$e := \sqrt{\Delta a_1^2 + \Delta a_2^2} \quad (8)$$

is chosen as an indication of observer performance.

III.4 Observer-based control

Figure 6 illustrates the structure of an observer-based control.

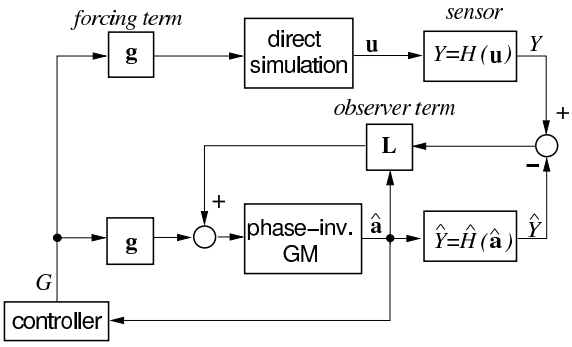

Figure 6: *Principal sketch of the observer-based control in the online phase.*

The direct simulation of the flow and the continuously updated observer system are evaluated simultaneously. The amplitude and sign of the volume force are calculated with the energy-based controller of Sec. III.2 and the estimated state vector $\hat{\mathbf{a}}$.

Figure 7 shows the transients of selected variables under observer-based control. The oscillation amplitude, A, decreases rapidly during the first three periods of control and after six periods A is stabilized at a lower level. The transient of the shift-mode amplitude a_Δ is very similar. The plots of both A and a_Δ show that the energy-based control input G, see Fig. 7 *(middle)*, leads to a reduction of the fluctuation energy.

Yet, complete suppression in the entire wake region cannot be achieved for two reasons. The most important cause is the intrinsic limitation of local actuation forces at highly supercritical Reynolds numbers, as has already been noted in similar studies.[13,17] The second limitation of control is the quality of the state-space estimation by the dynamic observer. The transient of e (Fig. 7, second sub-figure from bottom) shows an increase of the estimation error as the state-space variables move away from the natural limit cycle.

This growing uncertainty of the observer can be traced back to the fact that the estimation is based on Karhunen-Loève modes of the natural flow, which do not include changes of the flow structure caused by control. In the controlled state of the flow, the natural Karhunen-Loève modes resolve less fluctuation energy. It may be noted that the decrease of a_Δ indicates the growing length of the recirculation bubble of the mean flow (compare with Fig. 2), associated with corresponding spatial shifts in the leading oscillatory modes. Thus, the difference between the GA (3) and the real flow increases as the controlled flow leaves its natural, un-actuated limit cycle.

Close to the limit cycle, the energy-based controller gives rise to a force which counteracts the transverse fluid motion in the actuation region. Thus, the near-wake is stabilized. At this state, energy-based control is essentially opposition control. As actuation changes the flow structure, the phase relations between the velocity at the sensor position and at other locations are affected. In particular, the time shift between model-predicted and computed velocity in the actuation region implies that the transverse force does not always counteract the transverse fluid motion. Thus, model-based control becomes less efficient with reduced fluctuation level.

Figure 7 *(bottom)* shows the transient of the normalized fluctuation energy

$$K = \frac{1}{2}\iint_{\Omega_0} dx\,dy\,\mathbf{u}^*\cdot\mathbf{u}^* \quad (9)$$

where $\mathbf{u}^*$ denotes the difference between the velocity field $\mathbf{u}$ and the base flow $\mathbf{u}_B$,

$$\mathbf{u}^* := \mathbf{u} - \mathbf{u}_B\,, \quad (10)$$

$$\mathbf{u}_B := \mathbf{u}_s + a_\Delta\mathbf{u}_\Delta\,. \quad (11)$$

The base flow $\mathbf{u}_B$ is the projection of the velocity field on the line from the steady solution in shift-

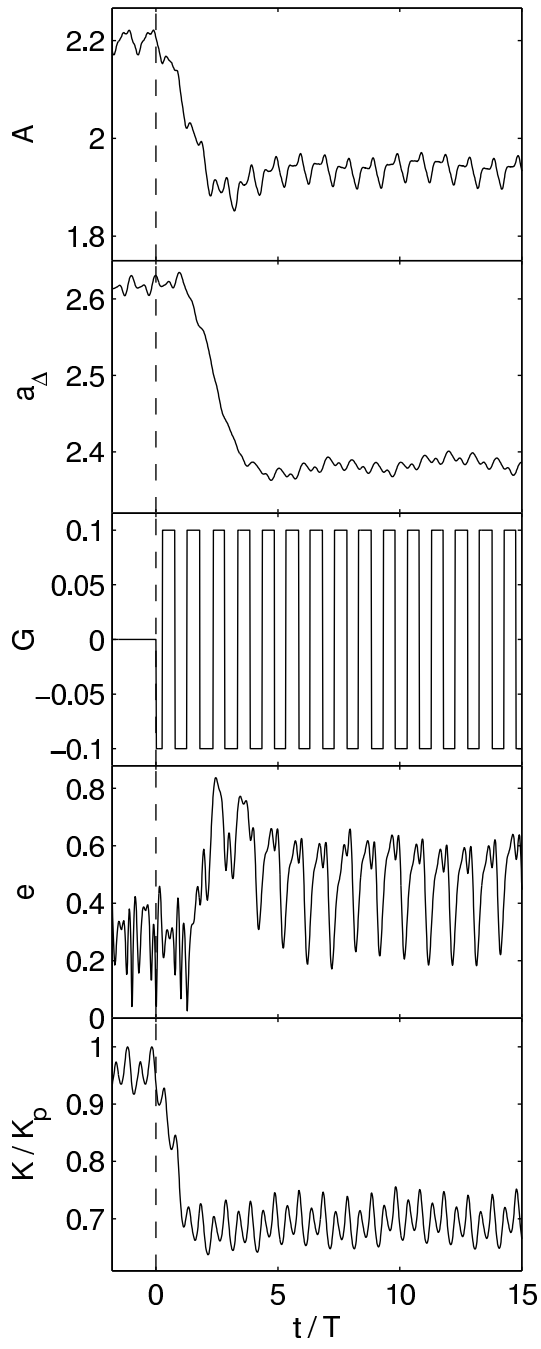

Figure 7: *Transient phase of the Navier-Stokes simulation employing the observer-based control. The control effects are monitored by the amplitude A of the oscillation, the shift-mode amplitude a_Δ, the amplitude G of the volume force, the observer error e and the normalized fluctuation energy K/K_p from top to bottom, respectively.*

mode direction $\mathbf{u}_\Delta$. It can be interpreted as the ensemble average over all phases. K_p in Fig. 7 is the kinetic energy of the natural periodic flow. The fluctuation energy is evaluated in the observation region

$$\Omega_0 := \{(x, y) : -5 \leq x \leq 6.5, |y| \leq 5\} \qquad (12)$$

The transient of K/K_p shows a fast decay of the fluctuation in the first two periods of control. Subsequently, the fluctuation energy is stabilized at a level that is 31% smaller than the level of the natural limit cycle. This percentage is compared with other strategies in Sec. IV.

The next three figures are used to analyze the qualitative and quantitative differences between the natural and the controlled flow. In Fig. 8, snapshots of the natural and the controlled flow are visualized. The damping effect of the actuation is most evident in the observation region. The oscillation amplitude is drastically reduced and the transverse fluid motion has been nearly suppressed in the near-wake.

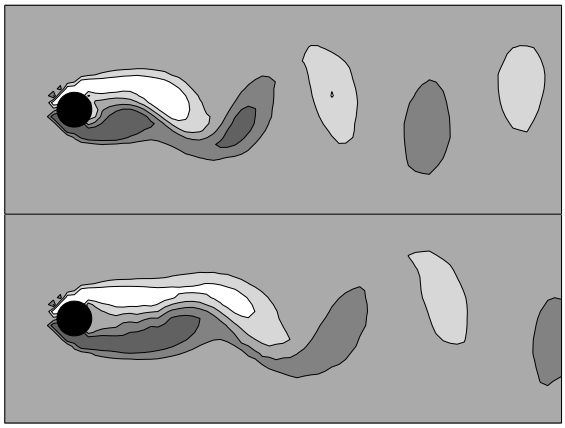

Figure 8: *Comparison of vorticity of the natural (top) and controlled flow (bottom). Brighter regions indicate positive values, darker regions negative values. The vortex shedding is damped in the observation region behind the cylinder*

Figure 9 shows the modification of the first Karhunen-Loève mode, when snapshots of the controlled flow are used for the GA. The iso-lines of the stream-function show a reduced activity in the near-wake and a change of the mode shape e.g. a longer streamwise wavelength. An empirical GM has also been constructed based on this new GA of the controlled flow. This modified system is in better agreement with the simulation at the controlled operating point.

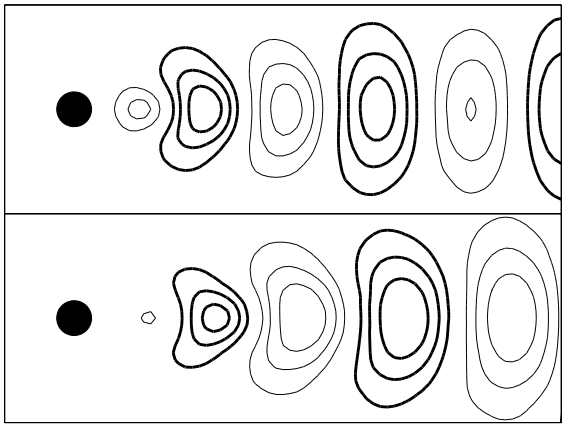

Figure 9: *First Karhunen-Loève mode of natural (top) and controlled flow (bottom). The modes are visualized by iso-contour lines of the stream-function. Positive values are indicated by thick lines, negative values by thin lines.*

The streamwise growth of fluctuation is characterized by the averaged density of the fluctuation energy $K(x)$,

$$K(x) = \frac{1}{2} \int_{-5}^{+5} dy \ \langle u^{*2} + v^{*2} \rangle \ , \qquad (13)$$

were $u(x,y,t)^*$ and $v(x,y,t)^*$ are the local values of $\mathbf{u}^*$ in Eq. (10). $\langle\ \rangle$ denotes the time average of the embraced term.

In Fig. 10, the energy densities, averaged over one period of the natural and controlled flow, are compared. The $K(x)$-curves corroborate the qualitative findings of Figs. 8 and 9. The largest damping effect of the fluctuation, due to control, is found in the first six diameters downstream from the cylinder. The influence of the actuation on the flow near the outflow region, at $x = 15$, is very small.

To improve state estimation, an alternative observer design is based on the GM of the controlled flow. As expected, this reduces the estimation error. This change entails an increase of damping of fluctuation energy from 31% to 45%.

III.5 Complete-information control

In complete-information control, the whole velocity field is assumed to be known at each instant. An observer for the state estimation is therefore not required. The Fourier coefficients a_i are determined by an integral over the computational domain,

$$a_i = \iint_{\Omega} dx\, dy \ \mathbf{u}_i \cdot (\mathbf{u} - \mathbf{u}_s) \, . \qquad (14)$$

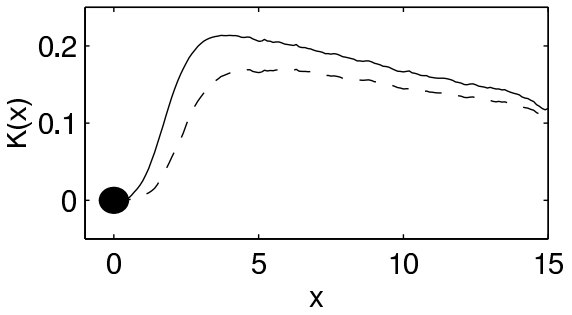

Figure 10: *Density of fluctuation energy $K(x)$ for the natural (—) and controlled (– –) flow. The influence of control is strongest in the near wake.*

Equation (14) can be considered the best-case reconstruction of state variables. The energy-based control using this state space information enables a reduction of the fluctuation energy in the observation region by 50%. Complete-information control is only feasible in numerical simulations, and cannot be practically implemented. It provides a useful benchmark for feasible performance with the postulated volume force actuation. In particular, our result indicates that the performance achieved with an observer-based compensation is very close to the best-case performance (45% vs. 50% attenuation).

III.6 An upper bound on performance

Passive vortex shedding suppression with a splitter plate in the near wake is used to compute yet another performance benchmark, against which one can compare the proposed model based control. The plate length is one cylinder diameter, and it is co-positioned with the volume-force field, downstream from the cylinder. A no-penetration condition is enforced at the splitter plate, setting the v-component of the flow to zero. The effect of the splitter plate on the u-component is neglected, since the volume force of the previously introduced active control has no direct influence on the u-component. In the observation region, the splitter plate reduces the fluctuation energy by 60%. The performance exceeds all other approaches. This is not surprising since the splitter plate can be envisioned as a high-dimensional row of distributed local volume forces each of which effectively inhibits transverse fluid motion with no observation and other errors.

IV Discussion of simulation results

Table 1 summarizes the results of flow control presented in the Secs. III.4–III.6. Beside the damping of the fluctuation it includes also variations of the vortex-shedding period. The control leads to an increase of the period which is consistent with the smaller Strouhal number near the steady solution of the wake flow.

Table 1: *Comparison of the different control strategies. The effect is monitored with the normalized averaged fluctuation energy $\bar{K}/\bar{K}_p$ and the period T.*

control strategy		$\bar{K}/\bar{K}_p$	T
no actuation		1.00	6.0
observer-based control	natural GM	0.69	6.0
	controlled GM	0.55	6.8
complete-information control		0.50	6.9
splitter plate		0.40	7.3

Performance of all three feedback policies is compared to the splitter-plate benchmark. The reduction of 31% with the observer-based control reaches about one half of that ideal level. It should be viewed against the backdrop of the fact that it is based on a GM whose original validity was restricted to the natural flow. Indeed, this level of performance was made possible only by the robustness gained with the added shift-mode.

Evidently, a challenging aspect of model-based flow control is the limitation of accurate predictions to the design operating points. Here, considered operating points are the natural flow and the controlled limit cycle. Performance is therefore improved to 45% suppression — or three quarters of the splitter-plate benchmark — when a model is matched on the target region, as opposed to a calibration on the original natural flow.

To some extent, the regime of model validity has been incorporated in the control by restricting controlled transients to the neighborhood of the center-manifold paraboloid (see Fig. 4). However, while it is always possible to stabilize the fixed point within the GM, that goal cannot be achieved with the actual system. The reason for this discrepancy is that a global Galerkin ansatz cannot accurately describe near- and far-wake coupling for all control points. The authority of the volume force on the Galerkin solution — represented by the coefficients g_i — vanishes in reality, close to the maximum achievable suppression of vortex shedding.

V Conclusions and outlook

A new approach is pursued for active flow control using low-dimensional Galerkin models (GM). A first proof of concept is presented for the volume-force actuated flow around a circular cylinder. The two key ingredients are the inclusion of the shift-mode, which enhances the dynamic range of model validity, and a controller design which respects this validity regime.

The presented strategy of GM-based control is further developed at the Collaborative Research Center (Sfb 557) "Control of Complex Turbulent Flow" at the Technical University Berlin and at Northeastern University. Considered configurations include several internal flows and local acoustic actuators. This approach synergizes with a corresponding strategy based on low-dimensional vortex models.[21]

Acknowledgments

The authors acknowledge funding and excellent working conditions of the Collaborative Research Center (Sfb 557) "Control of complex turbulent flow" supported by the Deutsche Forschungsgemeinschaft (DFG) and hosted at the Technical University Berlin. Bernd R. Noack acknowledges also funding of the DFG under grant NO 258/1-1. The work of Gilead Tadmor was supported by the U.S. National Science Foundation under grants ECS 0136404 and CCR 0208791. We acknowledge stimulating discussions with Konstantin Afanasiev, Stefan Siegel and Frank Thiele.

References

1. T.R. Bewley and S. Liu, "Optimal and robust control and estimation of linear paths to transition," J. Fluid Mech., vol. 365, pp. 305–349, 1998.

2. G.H. Cottet and P. Koumoutsakos, Vortex Methods — Theory and Practice. Cambridge University Press, Cambridge, 2000.

3. S. Narayanan, B.R. Noack and E. Meiburg, "Reduced-order dynamical modeling of sound generation from a jet," AIAA Paper 2002–0073, 40th Aerospace Sciences Meeting and Exhibit, 2002.

4. P.W. Holmes, J.L. Lumley and G. Berkooz, Turbulence, Coherent Structures, Dynamical Systems and Symmetry, Cambridge University Press, Cambridge, 1998.

5. B.R. Noack and H. Eckelmann, "A low-dimensional Galerkin method for the three-dimensional flow around a circular cylinder," Phys. Fluids, vol. 6, pp. 124–143, 1994.

6. M.F. Unal and D. Rockwell, "On the vortex formation from a cylinder; Part2. control by a splitter-plate interference," J. Fluid Mech., vol. 190, pp. 513–529, 1987.

7. P.J. Strykowski and K.R. Sreenivasan, "On the formation and suppression of vortex 'shedding' at low Reynolds numbers," J. Fluid Mech., vol. 218, pp. 71–107, 1990.

8. V.L. Zhdanov and H. Eckelmann, The effect of jet bleed on base pressure distribution, shedding frequency, and mean velocity profiles in the wake behind a two-dimensional blunt model, Mitteilung Nr. 9, Max-Planck-Institut für Strömungsforschung, 1990.

9. E. Detemple-Laake and H. Eckelmann, "Phenomenology of Kármán vortex streets in oscillatory flow," Exps. Fluids, vol. 7, pp. 217–227, 1989.

10. K. Roussopoulos, "Feedback control of vortex shedding at low Reynolds numbers," J. Fluid Mech., vol. 248, pp. 267–296, 1993.

11. M. Morzyński and F. Thiele, "Numerical stability analysis of a flow about a cylinder," Z. Angew. Math. Mech., vol. 71, pp. T424–T428, 1991.

12. H.–Q. Zhang, U. Fey, B.R. Noack, M. König and H. Eckelmann, "On the transition of the cylinder wake," Phys. Fluids A, vol. 7, pp. 779–794, 1995

13. K. Afanasiev, Stabilitätsanalyse, niedrigdimensionale Modellierung und optimale Kontrolle der Kreiszylinderumströmung (transl.: Stability analysis, low-dimensional modeling, and optimal control of the flow around a circular cylinder), PhD thesis, Fakultät Maschinenwesen, Technische Universität Dresden, 2003.

14. B.R. Noack, P. Papas and P. A. Monkewitz, Low-dimensional Galerkin model of a laminar shear-layer, Technical Report 2002-01, Laboratoire de Mecanique des Fluides, Departement de Genie Mecanique, Ecole Polytechnique Fédérale de Lausanne, 2002.

15. B.R. Noack, K. Afanasiev, M. Morzyński and F. Thiele, "A hierarchy of low-dimensional models for the transient and post-transient cylinder wake," accepted for publication in J. Fluid Mech., 2003.

16. A.E. Deane, I.G. Kevrekidis, G.E. Karniadakis and S.A. Orszag, "Low-dimensional models for complex geometry flows: Application to grooved channels and circular cylinders," Phys. Fluids A, vol. 3, pp. 2337–2354, 1991.

17. S. Siegel, K. Cohen and T. McLaughlin, "Feedback control of a circular cylinder wake in experiment and simulation," AIAA Paper 2003–3569, 33rd AIAA Fluids Conference and Exhibit, 2003.

18. G.S. Copeland and B.R. Noack, On the Landau equation for vortex shedding, Technical Report 02/2000, Hermann-Föttinger-Institut für Strömungsmechanik, Technische Universität Berlin, 2000.

19. B.R. Noack and G.S. Copeland, On a stability property of ensemble-averaged flow, Technical Report 03/2000, Hermann-Föttinger-Institut für Strömungsmechanik, Technische Universität Berlin, 2000.

20. G. Tadmor, B.R. Noack, A. Dillmann, M. Pastoor, J. Gerhard, R. King and M. Morzyński, "Control, observation and energy regulation of wake flow instabilities," submitted to 42nd IEEE Conference on Decision and Control, 2003.

21. M. Pastoor, R. King, B.R. Noack, A. Dillmann and G. Tadmor, "Model-based coherent-structure control of turbulent shear flows using low-dimensional vortex model," AIAA Paper 2003–4261, 33rd AIAA Fluids Conference and Exhibit.